LETTERS
PUBLISHED ONLINE: 3 NOVEMBER 2013 | DOI: 10.1038/NPHOTON.2013.286
nature photonics

Petahertz optical oscilloscope

Kyung Taec Kim[1], Chunmei Zhang[1], Andrew D. Shiner[1], Bruno E. Schmidt[2], François Légaré[2], D. M. Villeneuve[1] and P. B. Corkum[1]*

The time-dependent field of an electromagnetic pulse can be measured if there is a fast enough gate. For terahertz radiation, femtosecond photoinjection of free carriers into a semiconductor in the presence of the terahertz radiation can serve as the gate[1]. For visible or infrared radiation, attosecond photoionization of a gas target in the presence of the optical field is a direct analogue[2–8]. Here, we show that nonlinear optical mixing[9–13] in a medium in which attosecond pulses are being generated can also be used to measure the time-dependent field of an optical pulse. The gate is the phase accumulated by the recollision electron during the subcycle time interval between ionization and recombination. We show that the instantaneous field of an unknown pulse is imprinted onto the deflection of the attosecond extreme ultraviolet pulse using an all-optical set-up with a bandwidth up to 1 PHz.

It is now technically feasible to produce time-dependent electromagnetic waveforms of almost arbitrary shape in the ultraviolet or longer wavelength region[8,14–17]. This means that very large time-dependent forces can be applied to the charged components of matter on the natural timescale of their electronic response[7,18]. Complete measurement of such a time-dependent waveform requires subcycle temporal resolution[19]. In current methods[2–8], an isolated attosecond pulse is produced by an intense laser pulse interacting with an atomic or molecular gas. The attosecond pulses are then refocused onto a second target to produce photoelectrons in the presence of the signal field to be measured. The complete waveform of the light pulse is obtained from the momentum shift of the photoelectron spectrum caused by the signal field. This approach requires three complex technologies: photoelectron spectroscopy, extreme ultraviolet (XUV) focusing optics and a high flux source of attosecond pulses. Here, we demonstrate an all-optical technique to measure the waveform of the light pulse that requires only a low flux attosecond source and an XUV spectrometer. In other words, we remove the requirement for photoelectron spectroscopy, XUV focusing optics, and substantial flux in an attosecond beam.

Our approach uses the attosecond process that underlies attosecond pulse generation as the gate. To appreciate how, consider the three-step model of attosecond pulse generation shown in Fig. 1a[20]: (1) the strong fundamental laser field $E_0(t)$ liberates an electron at time t_i; (2) the electron propagates in the field until it recollides; and (3) it recombines with its parent ion at t_r. The electron path that produces the XUV photon at energy ε through the short quantum path[21] is illustrated with a red arrow in Fig. 1a. Because the excursion time of the electron $(t_r - t_i)$ is much shorter than one optical cycle of the visible light, this short electron path offers subcycle temporal resolution.

To access the gate, the unknown signal field $E_s(t)$ to be measured is added to the fundamental laser field $E_0(t)$. The signal field weakly perturbs the attosecond pulse generation process[9,10,13]. The electron trajectory that produces the XUV photon with energy ε is modified, as illustrated with a blue arrow in Fig. 1a. This perturbation changes the phase of the XUV radiation by σ_ε. It should be noted that the additional signal field influences the generation process only during the excursion time $(t_r - t_i)$. Thus, σ_ε is proportional to the averaged field strength of the signal field during the excursion time (see Supplementary Section 1 for details), which can be written approximately as

$$\sigma_\varepsilon(\tau) \propto E_s(\tau + \xi_\varepsilon)$$

where ξ_ε is a negligible constant time delay that depends only on ε.

We can simulate the single-atom response using a single set of recollision trajectories (short trajectories). Figure 1b–d presents calculation results for a neon atom. The XUV radiation is calculated using the strong field approximation[21–23]. The phase difference of the XUV radiation, with and without the signal field, is obtained as a function of the time delay between E_0 and E_s. In the figure, phase differences obtained at 39 eV, σ_{39eV}, are compared with the original signal pulse used in the calculation. These results confirm that the phase shift σ_ε is proportional to the signal field.

In an experiment, XUV radiation is produced in a distributed medium. A perturbation made to the fundamental beam can change the wavefront of the XUV radiation, leading to deflection of the XUV beam[13]. We use this macroscopic response to make the phase difference σ_ε observable by using a non-collinear experimental set-up (Fig. 2a). Because the signal beam is superimposed on the fundamental at a small angle θ_s, the atoms in the medium experience the signal field at slightly different times, depending on their vertical position y (Fig. 2b). This breaks the symmetry of the XUV phase along the vertical direction, and the propagation direction of the XUV radiation is changed. As shown in Supplementary Section 2, the propagation angle of the XUV radiation is proportional to the derivative of the signal field (that is, $\theta(\tau) \propto dE_s(t)/dt|_{t=\tau}$). The change of the propagation angle can be measured from the angularly resolved XUV spectrum, as shown in Fig. 2c.

By generalizing the single-atom model to distributed neon atoms, we illustrate the relation between the propagation angle and the signal field. The XUV radiation is calculated using the strong field approximation[21–23] from a 250-μm-long neon medium placed at the focus. The angular distribution of the XUV radiation is obtained by propagating the XUV radiation to the far-field (see Methods for details). We used three different signal waveforms (triangle, chirped Gaussian cosine and chirped Gaussian sine pulses). The angular distribution of the XUV emission (vertical line-out of the spectrum) at 39 eV as a function of the time delay τ is shown in Fig. 2d–f. The calculated angular distribution agrees with the derivative of the original signal field (solid lines, Fig. 2d–f).

For an experimental demonstration of waveform measurement we use 750 nm Ti:sapphire laser pulses. The laser beam is split into two beams. One beam is used as the fundamental E_0, generating an attosecond XUV pulse. The polarization gating technique selects a single recollision from neon[5]. The other beam, E_s, is the pulse to

[1]Joint Attosecond Science Laboratory, University of Ottawa and National Research Council, 100 Sussex Drive, Ottawa, Ontario K1A 0R6, Canada, [2]INRS-Énergie et Matériaux, 1650 boulevard Lionel-Boulet, C.P. 1020, Varennes, Québec J3X 1S2, Canada. *e-mail: paul.corkum@nrc-cnrc.gc.ca

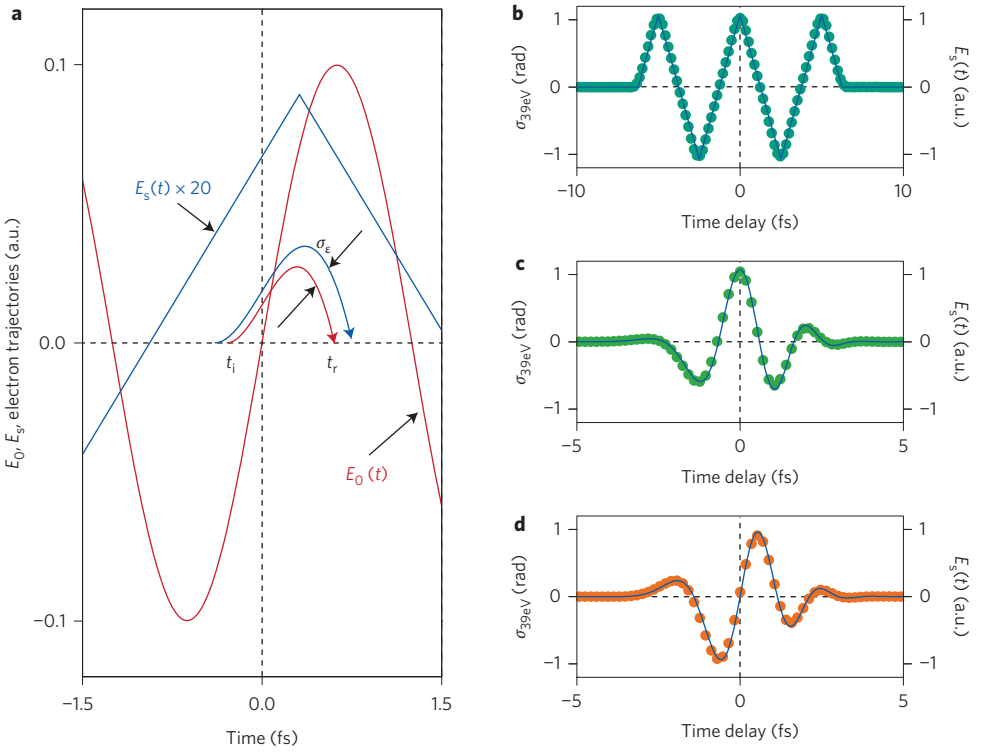

Figure 1 | Basic idea of the petahertz optical oscilloscope. a, Illustration of electron trajectories. The electron trajectory calculated from a single neon atom by the driving laser pulse $E_0(t)$ with an intensity of 3.5×10^{14} W cm^{-2} is shown with a thick red line with an arrow head. The modified electron trajectory is shown with a thick blue line with an arrow head when the weak signal field $E_s(t)$ is added. **b**–**d**, Phase shift of the XUV radiation for different signal fields. The XUV phases are calculated with and without the signal field as a function of the time delay between E_0 and E_s. Their phase differences at 39 eV are shown with circles for the triangle pulse (**b**), chirped Gaussian cosine pulse (**c**) and chirped Gaussian sine signal pulse (**d**). The original signal pulses used in the calculations are shown as blue lines.

be measured (see Methods for experimental details). The quasi-continuum XUV spectrum obtained from the fundamental beam is shown in Fig. 3a. The spectral modulation of 0.2, $(I_{MAX} - I_{MIN})/(I_{MAX} + I_{MIN})$, near 39 eV remains due to the pre- and post-XUV pulses near the single XUV pulse. According to the simulation shown in Fig. 2 where the same amount of the spectral modulation is considered, it does not affect our measurement.

Figure 3b shows the angular distribution measured at 39 eV as a function of time delay. The average propagation angle (white line), found by fitting with a Gaussian distribution, is the derivative of the signal laser field. The measurement shows a 5.1 fs pulse containing two optical cycles in a central peak, with weaker signal stretching before and after the main pulse. The spectrum obtained by taking the Fourier transform of the signal field qualitatively agrees with the spectrum measured by a grating spectrometer (Fig. 3c). Although our technique determines the spectrum of the actual pulse measured over a limited time window, the spectrum measured by the grating-based spectrometer shows all spectral components, including parts that do not contribute to the main pulse. This fundamental difference accounts for some of the discrepancy between the two spectra.

The temporal resolution of the measurement is related to the excursion time (900 as for 39 eV) of the recollision electron in the continuum. If the signal field oscillates too fast compared to the excursion time, the effect of the signal field on the electron trajectory will average out. Averaging limits the measurable wavelength of the signal field. To estimate the lowest wavelength that can be measured, we calculate the spectral response of the measurement $|\sigma_{39eV}|^2$ with a sinusoidal signal field for different wavelengths. The amplitude of $|\sigma_{39eV}|^2$ is shown with a green dashed line in Fig. 3c. As we decrease the wavelength of the signal field, the amplitude also decreases. However, we find that the optical period of the shortest measurable wavelength is below the excursion time. Using only a single quantum trajectory, a signal with a wavelength of 200 nm (1.5 PHz) or longer could be measured with our 760 nm fundamental. Using more trajectories, the resolution could be improved. This temporal resolution is an intrinsic property of the highly nonlinear process of high harmonic generation. It is not changed by dispersion of the attosecond pulse after generation. Therefore, our approach to measurement does not require chirp control of the attosecond pulse[24,25].

To verify that we determine the time-dependent electric field, we measured five waveforms for different carrier envelope phases (CEPs), as shown in Fig. 4. The CEP of the signal pulse is controlled by adjusting a glass wedge without changing the fundamental pulse. The wedge changes the CEP as well as the relative phase between the fundamental and signal laser pulse. We fit the measured signal field with a Gaussian function as explained in the Methods, independently determining the delays (τ_0), durations (τ_{FWHM}), frequencies (ω_0) and CEP (Φ_{CEP}) for each waveform. The pulse durations and CEPs are summarized in each panel of Fig. 4. The full-width at half-maximum (FWHM) duration of the intensity is 4.8–5.0 fs. The standard deviations for each CEP measurement are 0.1–0.3 rad.

As we have emphasized, adding the signal field at an angle modifies the XUV phase along the vertical directions. With a small angle, the signal field imposes a slowly changing phase gradient that changes the propagation angle (first-order phase) of the XUV beam. However, the phase gradient may also change the divergence (second-order phase) of the XUV beam, depending on the angle between the two laser beams and the intensity of the signal beam. The change of the divergence results in the asymmetric angular distribution shown in Figs 3b and 4. The angular distribution is broader when the waveform $(dE_s(t)/dt)$ rises than when it falls.

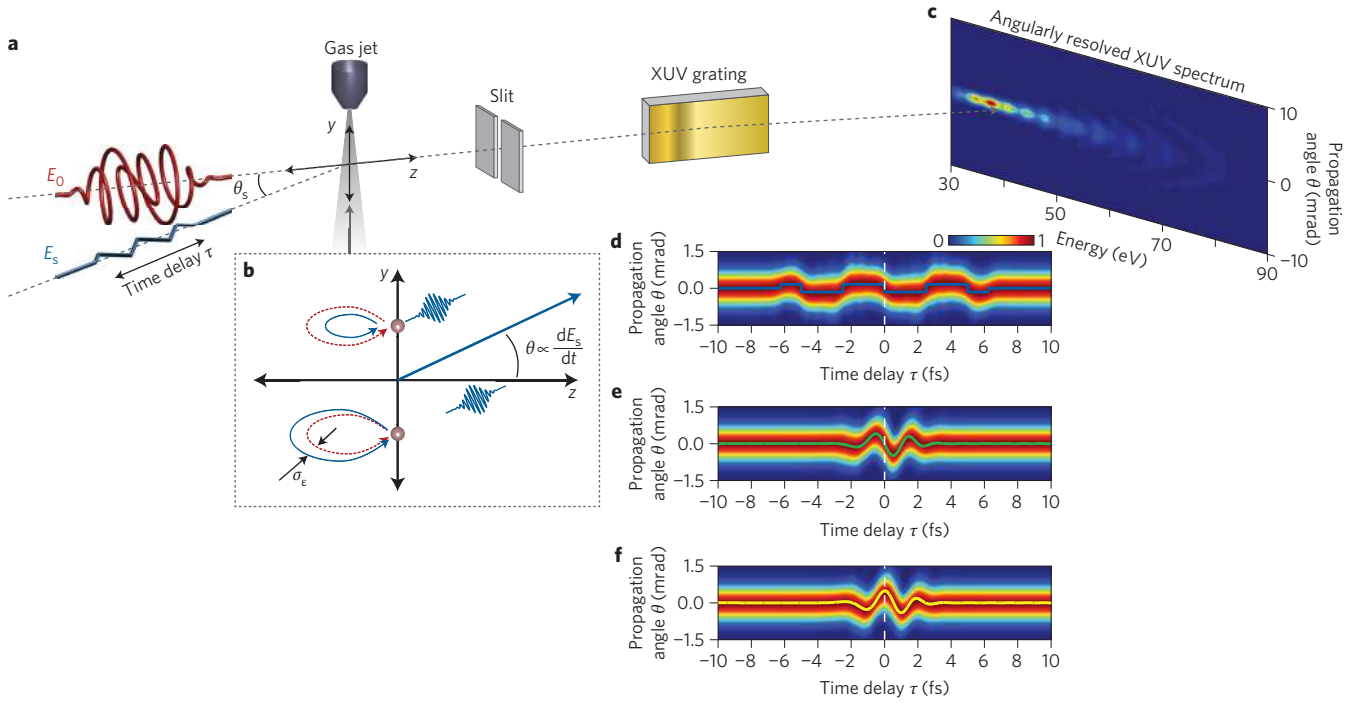

Figure 2 | Schematic set-up of the petahertz optical oscilloscope and theoretical calculations. a, Schematic set-up for the calculation and the experiment. The fundamental laser pulse $E_0(t)$ generates XUV radiation through high harmonic generation using the polarization gating technique. The signal laser pulse $E_s(t)$ is superposed with a small angle θ_s in the medium. **b**, Illustration of electron trajectories with (blue line with an arrow head) and without (red dotted line with an arrow head) the signal field. The propagation angle of the XUV radiation is illustrated with a thick blue line with an arrow head. **c**, Angularly resolved XUV spectrum, where the spectrum is calculated from the 250-μm-long neon medium placed at the focus with a central wavelength of 750 nm and an intensity of 3.5×10^{14} W cm^{-2}. A single XUV pulse is selected with the pre- and post-pulses to yield a spectral modulation of 0.2 (see Methods for details). **d**–**f**, Angular distribution (vertical lineouts) of the XUV spectrum at 39 eV calculated as a function of the time delay τ for various signal fields: the triangle (**d**), the chirped Gaussian cosine (**e**) and the chirped Gaussian sine (**f**) pulses. The intensity of the signal fields is 7×10^{11} W cm^{-2}. For comparison, the derivative of the original signal field used in the calculations, $dE_s(t)/dt$, is shown as solid lines.

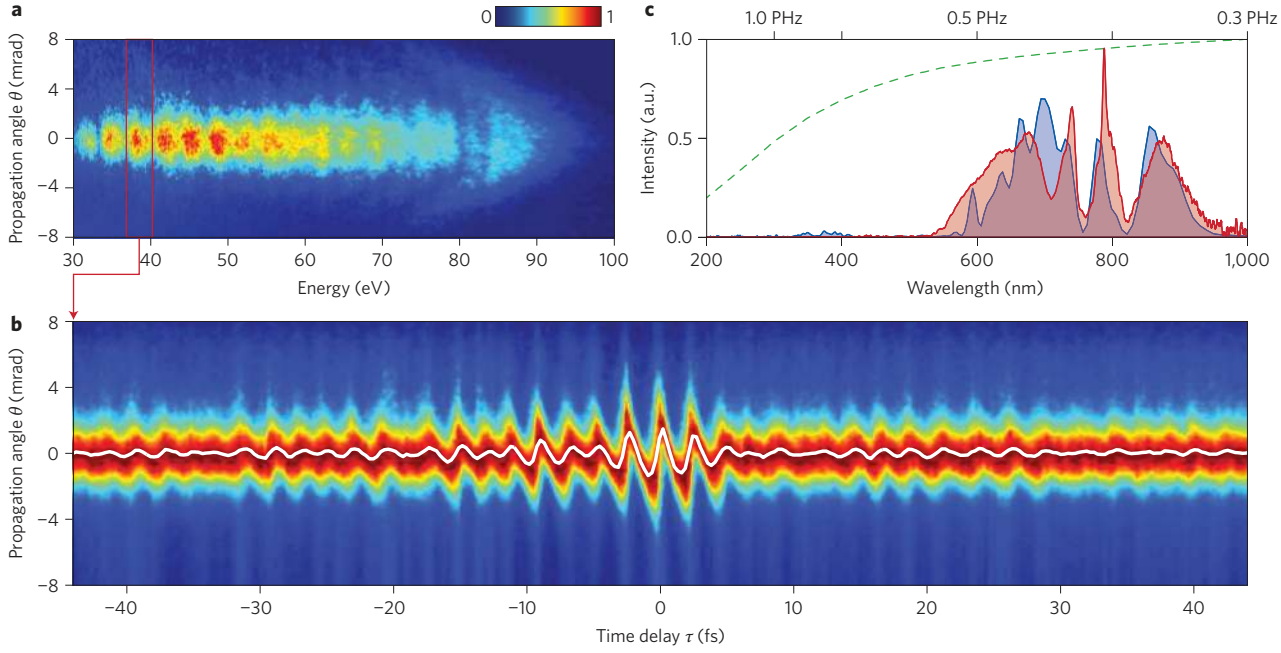

Figure 3 | Waveform measurement of few-cycle pulses. a, Experimental XUV spectrum obtained with the polarization gating technique. **b**, Normalized angular distribution of the XUV spectrum for the range marked with the red box near 39 eV as a function of time delay τ. The centre of mass that corresponds to the derivative of the electric field, $dE_s(t)/dt$, is shown with a white solid line. **c**, Spectrum of the signal laser pulse obtained from $E_s(t)$ measured in **b** (blue line). The spectrum measured by a grating-based spectrometer (red line) is also shown for comparison. The spectral sensitivity of the measurement technique is shown with a green dashed line (normalized by the amplitude at 1 μm).

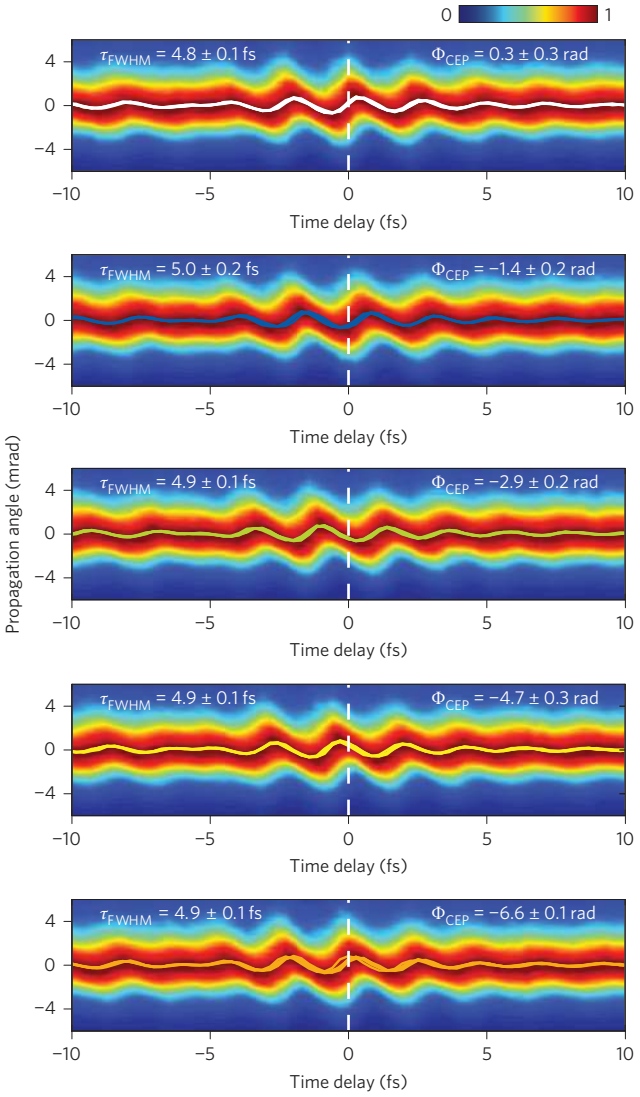

Figure 4 | Waveform measurement of few-cycle pulses with different CEPs. The waveforms are measured five times for five different CEPs to show the reproducibility of the measurements. The colour code shown in each panel is the first angular distribution of the five measurements. Five waveforms in each panel are shown with solid lines. The average durations and CEPs are summarized in each panel.

In the case of Fig. 3, this asymmetry causes a 4% artificial second harmonic (near 370 nm), as shown in Fig. 3c.

The asymmetry of the measurement can be improved by reducing the angle between two laser beams or the intensity of the signal pulse, or it can be avoided by using the phase retrieval technique to find the phase gradient in the near-field[13]. Alternatively, the phase shift imposed by the signal field can be measured in a two-XUV-source interference experiment[26–29] in which the signal pulse is co-linearly added in one of the two fundamental laser beams. The phase shift imposed by the signal pulse can be found by measuring the shift of the fringe pattern at the far-field (see Supplementary Section 3 for details).

In the current experimental set-up where the signal field is added at a small angle to deflect the XUV beam, multiple measurements at different τ are required to determine the waveform of the signal field. However, our approach is compatible with single-shot measurement of the time-dependent waveform. Consider the case where the weak signal pulse travels perpendicular to the fundamental beam and is spatially smaller than the transverse dimensions of the fundamental beam. If the polarizations of the beams are parallel, then the spatially dependent phase modulation caused by the signal beam creates a transient grating[10,26,29] that diffracts the XUV radiation. Depending on the absolute phase of the signal field, the position of the grating will be changed, so the phase of the XUV angular distribution is also changed at the far-field. The signal field is fully determined by the amplitude and phase measured in the far-field[27]. Single-shot measurements will be especially valuable for light sources that have an unstable CEP, such as high-peak-power lasers or low-repetition-rate lasers.

In conclusion, we have demonstrated an all-optical technique for measuring arbitrary waveforms of optical pulses. Our method can be applied to any wavelength longer than ~200 nm. It exploits the highly nonlinear process of high-harmonic or attosecond pulse generation. The attosecond pulse serves as an observable of the subcycle interaction. We expect that other highly nonlinear interactions hold the prospect of attosecond gating. However, even without refinement, our measurement is fast, compact and efficient.

Methods

We used a CEP-stabilized 5 fs, 760 nm Ti:sapphire laser pulse. The CEP stability was 400 mrad (root mean square). The laser beam was divided by a mirror with a small hole in the centre. The reflected beam was used as a fundamental beam for high harmonic generation. The reflected beam passed through a 120-μm-thick quartz plate and a broadband quarter-wave plate to create a beam for polarization gating[5]. The small beam passing through the hole was used as a signal beam. Two beams were combined at the focus with an angle of $\theta_s = 21$ mrad. The time delay between two beams was controlled by a piezo stage. The positive time delay means that the signal pulse precedes the fundamental pulse.

XUV radiation was obtained as a neon supersonic gas jet placed at the focus (nozzle diameter of 250 μm with a backing pressure of 6 bar). The medium length was estimated to be 250 μm. The intensities of the fundamental and signal laser pulses were 3.5×10^{14} W cm^{-2} and 3.5×10^{12} W cm^{-2}, respectively. The angular distribution shown in Fig. 3 was obtained by integrating over the energy range from 36.9 eV to 40.2 eV for each time delay. The propagation angle was obtained from the centre of mass calculated by fitting the angular distribution with a Gaussian distribution. To determine the pulse parameters shown in Fig. 4, the signal field was fitted by a Gaussian pulse as

$$E_s(\tau) = A_0 \exp\left[-2\log 2\frac{(\tau-\tau_0)^2}{\tau_{FWHM}^2}\right]\cos[\omega_0(\tau-\tau_0)+\Phi_{CEP}]$$

where A_0, τ_0, τ_{FWHM}, ω_0 and Φ_{CEP} are the amplitude, the delay, the duration, the angular frequency and the CEP of the laser pulse. The size of the fundamental beam was 30 μm (FWHM), and the signal beam was larger than 100 μm.

For the simulation results shown in Fig. 2, we used the strong field approximation model to calculate the XUV radiation from the 250-μm-long neon medium placed at the focus[13,21–23]. A single XUV pulse was selected, with pre- and post-pulses, to yield a spectral modulation of 0.2. The spectral modulation is defined as $(I_{MAX} - I_{MIN})/(I_{MAX} + I_{MIN})$ near 39 eV. The propagation of both the XUV and fundamental laser pulses through the medium was considered, but the distortion of the laser pulse due to plasma formation was not considered due to the low ionization rate of neon.

Received 21 May 2013; accepted 25 September 2013; published online 3 November 2013

References

1. Ferguson, B. & Zhang, X.-C. Materials for terahertz science and technology. *Nature Mater.* **1,** 26–33 (2002).
2. Itatani, J. *et al.* Attosecond streak camera. *Phys. Rev. Lett.* **88,** 173903 (2002).
3. Goulielmakis, E. *et al.* Direct measurement of light waves. *Science* **305,** 1267–1269 (2004).
4. Mairesse, Y. & Quéré, F. Frequency-resolved optical gating for complete reconstruction of attosecond bursts. *Phys. Rev. A* **71,** 011401 (2005).
5. Sansone, G. *et al.* Isolated single-cycle attosecond pulses. *Science* **314,** 443–446 (2006).
6. Mashiko, H. *et al.* Double optical gating of high-order harmonic generation with carrier-envelope phase stabilized lasers. *Phys. Rev. Lett.* **100,** 103906 (2008).
7. Goulielmakis, E. *et al.* Real-time observation of valence electron motion. *Nature* **466,** 739–743 (2010).
8. Wirth, A. *et al.* Synthesized light transients. *Science* **334,** 195–200 (2011).
9. Dudovich, N. *et al.* Measuring and controlling the birth of attosecond XUV pulses. *Nature Phys.* **2,** 781–786 (2006).

10. Bertrand, J. B. *et al.* Ultrahigh-order wave mixing in noncollinear high harmonic generation. *Phys. Rev. Lett.* **106,** 023001 (2011).
11. Dahlström, J., L'Huillier, A. & Mauritsson, J. Quantum mechanical approach to probing the birth of attosecond pulses using a two-colour field. *J. Phys. B* **44,** 095602 (2011).
12. Shafir, D. *et al.* Resolving the time when an electron exits a tunnelling barrier. *Nature* **485,** 343–346 (2012).
13. Kim, K. T. *et al.* Manipulation of quantum paths for space–time characterization of attosecond pulses. *Nature Phys.* **9,** 159–163 (2013).
14. Shverdin, M., Walker, D., Yavuz, D., Yin, G.-Y. & Harris, S. E. Generation of a single-cycle optical pulse. *Phys. Rev. Lett.* **94,** 033904 (2005).
15. Krauss, G. *et al.* Synthesis of a single cycle of light with compact erbium-doped fibre technology. *Nature Photon.* **4,** 33–36 (2009).
16. Huang, S. *et al.* High-energy pulse synthesis with sub-cycle waveform control for strong-field physics. *Nature Photon.* **5,** 475–479 (2011).
17. Chan, H. *et al.* Synthesis and measurement of ultrafast waveforms from five discrete optical harmonics. *Science* **331,** 1165–1168 (2011).
18. Kling, M. *et al.* Control of electron localization in molecular dissociation. *Science* **312,** 246–248 (2006).
19. Trebino, R. Measuring the seemingly immeasurable. *Nature Photon.* **5,** 189–192 (2011).
20. Corkum, P. B. Plasma perspective on strong field multiphoton ionization. *Phys. Rev. Lett.* **71,** 1994–1997 (1993).
21. Lewenstein, M., Salières, P. & L'Huillier, A. Phase of the atomic polarization in high-order harmonic generation. *Phys. Rev. A* **52,** 4747 (1995).
22. Yakovlev, V. S., Ivanov, M. & Krausz, F. Enhanced phase-matching for generation of soft X-ray harmonics and attosecond pulses in atomic gases. *Opt. Express* **15,** 15351–15364 (2007).
23. Yudin, G. L. & Ivanov, M. Y. Nonadiabatic tunnel ionization: looking inside a laser cycle. *Phys. Rev. A* **64,** 013409 (2001).
24. Kim, K. T., Kim, C. M., Baik, M. G., Umesh, G. & Nam, C. H. Single sub-50-attosecond pulse generation from chirp-compensated harmonic radiation using material dispersion. *Phys. Rev. A* **69,** 051805 (2004).
25. López-Martens, R. *et al.* Amplitude and phase control of attosecond light pulses. *Phys. Rev. Lett.* **94,** 033001 (2005).
26. Mairesse, Y. *et al.* High-order harmonic transient grating spectroscopy in a molecular jet. *Phys. Rev. Lett.* **100,** 143903 (2008).
27. Austin, D. R. *et al.* Lateral shearing interferometry of high-harmonic wavefronts. *Opt. Lett.* **36,** 1746–1748 (2011).
28. Bertrand, J. B., Wörner, H. J., Salières, P., Villeneuve, D. M. & Corkum, P. B. Linked attosecond phase interferometry for molecular frame measurements. *Nature Phys.* **9,** 174–178 (2013).
29. Smirnova, O. *et al.* High harmonic interferometry of multi-electron dynamics in molecules. *Nature* **460,** 972–977 (2009).

Acknowledgements

The authors thank D. Crane and B. Avery for technical assistance. The authors also acknowledge financial support from Canada's NRC (National Research Council of Canada) and NSERC (Natural Sciences and Engineering Research Council of Canada), the US AFOSR (Air Force Office of Scientific Research) and the DARPA (Defense Advanced Research Projects Agency) PULSE (Program in Ultrafast Laser Science and Engineering) programme through a grant by AMRDEC (the US Army Aviation and Missile Research, Development and Engineering Center).

Author contributions

K.T.K. conceived the idea. F.L., D.M.V. and P.B.C. supervised the project. K.T.K., C.Z., A.D.S. and B.E.S. performed the experiment and collected the data. K.T.K analysed the experimental data. K.T.K. and D.M.V. provided the numerical analysis. All authors contributed in writing the manuscript.

Additional information

Supplementary information is available in the online version of the paper. Reprints and permissions information is available online at www.nature.com/reprints. Correspondence and requests for materials should be addressed to P.B.C.

Competing financial interests

The authors declare no competing financial interests.

nature photonics

SUPPLEMENTARY INFORMATION

DOI: 10.1038/NPHOTON.2013.286

Supplementary Information on Petahertz Optical Oscilloscope

Kyung Taec Kim[1], Chunmei Zhang[1], Andrew D. Shiner[1], Bruno Schmidt[2], François Légaré[2], D. M. Villeneuve[1] and P. B. Corkum[1]

[1]Joint Attosecond Science Laboratory, National Research Council and University of Ottawa, 100 Sussex Drive, Ottawa ON K1A 0R6, Canada

[2]INRS-Énergie et Matériaux, 1650 boul. Lionel-Boulet, C.P. 1020, Varennes, Québec, J3X 1S2, Canada

September 18, 2013

In this supplementary information, we provide mathematical details discussed in the main paper "Petahertz Optical Oscilloscope". In Sec. 1, we derive an equation that describes a phase shift of XUV radiation induced by adding a weak additional field in high harmonic generation process. It is shown that the phase shift is linearly proportional to the electric field of the additional field. In Sec. 2, we show that the propagation angle of the XUV radiation is proportional to the derivative of the additional field. In Sec. 3, the distortion of the measured waveform is discussed. We also show how the distortion problem can be suppressed or eliminated.

1 Phase of XUV radiation with an weak additional laser pulse

High harmonic generation occurs when atoms or molecules are interacting with an intense fundamental laser field $\mathbf{E_0}(t)$, leading to the emission of XUV radiation. The spectral phase of the XUV radiation, ϕ_ε, at the photon energy ε can be written as

$$\phi_\varepsilon = -S_\varepsilon + \omega_\varepsilon t_r. \tag{S1}$$

Here, ω_ε is the angular frequency. S_ε is the quasi-classical action which is defined as [1]

DOI: 10.1038/NPHOTON.2013.286

$$S_\varepsilon = \int_{t_i}^{t_r} \left[\frac{\mathbf{v_0}(t)^2}{2} + I_p \right] dt. \tag{S2}$$

Here, $\mathbf{v_0}(t)$ is the instantaneous momentum of the electron. t_i and t_r are the ionization and the recombination time. We add an weak signal field $\mathbf{E_s}(t)$ with a time delay τ in the high harmonic generation, which changes the quasi-classical action S'_ε, ionization time t'_i, and recombination time t'_r, resulting in the phase shift of the XUV radiation. The phase shift σ_ε induced by adding the signal field can be obtained as

$$\sigma_\varepsilon(\tau) = \phi'_\varepsilon - \phi_\varepsilon = -(S'_\varepsilon - S_\varepsilon) + \omega_\varepsilon(t'_r - t_r). \tag{S3}$$

We numerically solve Eq. S3 with various signal fields such as a triangle, chirped Gaussian cosine and sine waveform. The calculation results summarized in Fig. 1 of the main paper confirm that the phase shift is linearly proportional to the signal field.

In this section, we provide an analytic description of the relation between the phase shift and the signal field. For the sake of simplicity, we ignore the ionization potential in Eq. S2. We also assume that the signal intensity I_s is much weaker than the fundamental intensity I_0. In the experiment, the ratio I_s/I_0 was 0.01. Then, the phase shift induced by adding the signal field can be written as [2]

$$\sigma_\varepsilon(\tau) = \int_{t_i}^{t_r} \left[\mathbf{v_0}(t) \int_{t_i}^{t} \mathbf{E_s}(t'+\tau) \mathrm{d}t' \right] \mathrm{d}t. \tag{S4}$$

Here, τ is the time delay between $\mathbf{E_0}$ and $\mathbf{E_s}$. We consider the harmonic generation process that produces a low energy photon through a short quantum path as shown in Fig. S1a. The harmonic generation occurs near $t = 0$ where the electric field can be approximated to be linear as $\mathbf{E_0}(t) = E_0 \sin(\omega_0 t) \approx E_0 \omega_0 t$. Then, the electron momentum can be approximated as shown in Fig. S1a as

$$\mathbf{v_0}(t) \approx -\frac{E_0 \omega_0}{2}(t^2 - t_i^2). \tag{S5}$$

Also, the ionization time t_i and the recombination time t_r are related as shown in Fig. S1b by

$$t_i \approx -t_r/2. \tag{S6}$$

Assuming the signal field is slowly varying from t_i to t_r, the signal field can be approximated to the first order near $t = \xi_\varepsilon$ as

$$\mathbf{E_s}(t) \approx E_s(\xi) + \left. \frac{dE_s}{dt} \right|_{t=\xi_\varepsilon} (t - \xi_\varepsilon). \tag{S7}$$

When $\xi_\varepsilon = 2t_r/5$, the first order term of Eq. S7 averages out in Eq. S4. Using Eq. S5-S7, Eq. S4 becomes

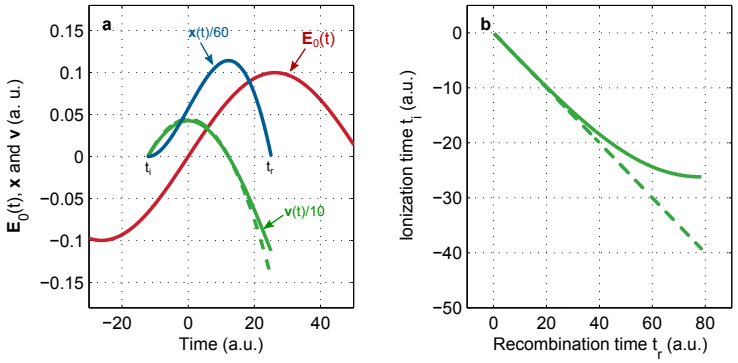

Figure S1: **Electron trajectory calculated with the SFA model and its approximation. a**, Electron trajectories are calculated from a Ne atom with a wavelength of 760 nm and an intensity of 3.5×10^{14} W/cm^2. The fundamental laser field $\mathbf{E_0}(t)$ is shown with a red solid line. The electron trajectory $\mathbf{x}(t)$ (a blue solid line) and the momentum of the electron $\mathbf{v}(t)$ (a green solid line) are calculated with the SFA model. The approximated momentum, $\mathbf{v}(t) \approx -E_0\omega_0(t^2 - t_i^2)/2$, is shown with the green dashed line. **b**, The recombination time and the ionization time are calculated with the SFA model (a green solid line). The approximated relation, $t_i \approx -t_r/2$, is shown with a green dashed line.

$$\sigma_\varepsilon(\tau) = \frac{9}{128} E_0\omega_0 t_r^4 E_s(\tau + \xi_\varepsilon). \tag{S8}$$

The additional delay ξ_ε is negligible because it is a constant delay that depends only on the recombination time (or XUV energy) [2].

2 Propagation angle of XUV radiation

The propagation angle of XUV radiation is determined by the XUV phase along the transverse direction in the medium. For the sake of simplicity, we consider only two atoms distributed along the vertical direction near $y = 0$. The signal field is added with a small angle θ_s as shown in Fig. S2. The effective time delay $\tau^\pm$ between two fields is different for two atoms depending on their positions. The time delay for the upper atom located at $+\Delta y$ is

$$\tau^+ = \tau + \Delta y\theta_s/c, \tag{S9}$$

and the delay for the lower atom located at $-\Delta y$ is

$$\tau^- = \tau - \Delta y\theta_s/c. \tag{S10}$$

DOI: 10.1038/NPHOTON.2013.286

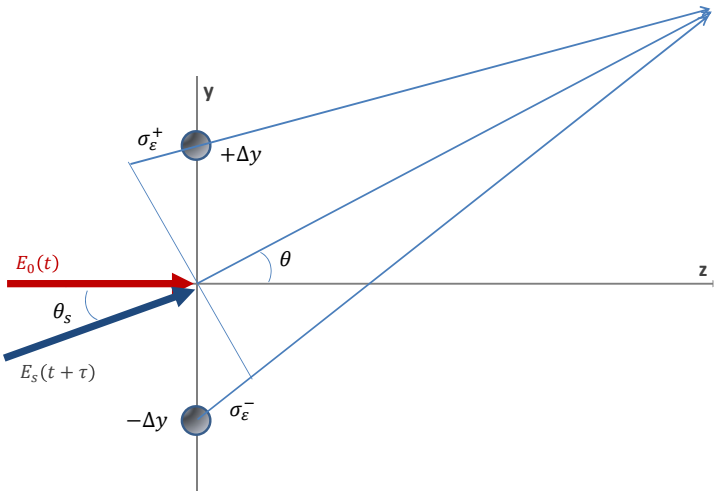

Figure S2: **Illustration of the XUV propagation angle.** Two atoms are distributed along the vertical direction at $+\Delta y$ and $-\Delta y$. Two laser beams are overlapped with a small angle θ_s. The phase shift of the XUV radiation for two atoms are σ_ε^+ and σ_ε^-. The propagation angle of the XUV radiation is θ.

Here, c is the speed of the light. τ is the time delay at $y = 0$. The phase shifts of the XUV radiation for each of these two atoms are

$$\sigma_\varepsilon^+ \propto E_s(\tau + \Delta y\theta_s/c) = E_s(\tau) + \frac{dE_s}{d\tau}\frac{\Delta y\theta_s}{c} + \ldots, \tag{S11}$$

, and

$$\sigma_\varepsilon^- \propto E_s(\tau - \Delta y\theta_s/c) = E_s(\tau) - \frac{dE_s}{d\tau}\frac{\Delta y\theta_s}{c} + \ldots. \tag{S12}$$

The propagation angle of the XUV radiation is proportional to the derivative of the signal field as

$$\theta(\tau) \approx \frac{k_y}{k_z} = \frac{1}{k_z}\frac{\sigma_\varepsilon^+ - \sigma_\varepsilon^-}{2\Delta y} \tag{S13}$$

$$\propto \frac{dE_s(\tau)}{d\tau}. \tag{S14}$$

3 Distortion of the measured waveform

In Sec. 2, the propagation angle is derived by considering only two atoms. In the distributed atoms, the phase of the XUV radiation - wavefront - contin-

uously varies. Due to the intensity-dependent harmonic phase, the wavefront of the XUV radiation is curved [1, 3]. When the oscillating signal pulse is superimposed on the fundamental driving laser pulse, the sinusoidal modulation is imposed on the curved XUV wavefront. This modulation may change not only the propagation angle (1st order phase) but also the divergence (2nd order phase) of the XUV radiation depending on the angle between two laser beams and the intensity of the signal beam [4]. The change of the divergence distorts the angular distribution, resulting in the asymmetric modulation. As shown in Fig. S3a-c, the angular distribution of the XUV radiation is broader when the $\mathrm{d}E/\mathrm{d}t$ rises, and thinner when the $\mathrm{d}E/\mathrm{d}t$ falls down.

In order to read the change of the propagation direction from the XUV angular distribution, we have fit the distribution with Gaussian. However, the measured waveform is still slightly asymmetric. This asymmetry introduces an artificial second and third harmonics as shown with a red line in Fig. S3d. In the case of Fig. 3c in the manuscript, the artificial second harmonics is about 4%. The artificial harmonic could be a serious problem when the signal pulse has more than one octave bandwidth. The distortion of the measurement can be reduced or completely avoided in different ways described below.

3.1 Use of small angle or low intensity signal field

Since the asymmetric waveform is caused by the higher-order modification of the XUV wavefront, it can be reduced by decreasing the angle between two laser beams or the intensity of the signal field. The latter is studied by the SFA model as shown in Fig. S3b. The waveform found by fitting the angular distribution with Gaussian is slightly distorted. Its spectrum contains 3% of an artificial second harmonic as shown with a red line in Fig. S3d. Figure S3c is the same calculation with a reduced intensity of $1.8 \times 10^{11}\mathrm{W/cm}^2$. The measured waveform is more symmetric. The artificial second harmonic is reduced to 0.5% (a blue line) which is comparable to noise level in our experiment. These calculations show that the distortion of the measured waveform can be reduced by adjusting the intensity of the signal pulse. (Note: In the SFA model the quadratic phase is weaker than we observe in the experiment. Therefore, we show results for slightly higher energy photons (49 eV) and a slightly more intense signal pulse ($1.8 \times 10^{12}\mathrm{W/cm}^2$).

3.2 Use of the phase-retrieval technique

We have used Gaussian fitting to find the propagation angle of the XUV radiation. However, there is a better way. We have used a phase retrieval algorithm to reconstruct the attosecond XUV pulse [4]. One can apply the similar technique to retrieve the phase modulation imposed by the signal field in the near-field. The phase retrieval algorithm will accurately reconstruct the waveform without distortion.

DOI: 10.1038/NPHOTON.2013.286

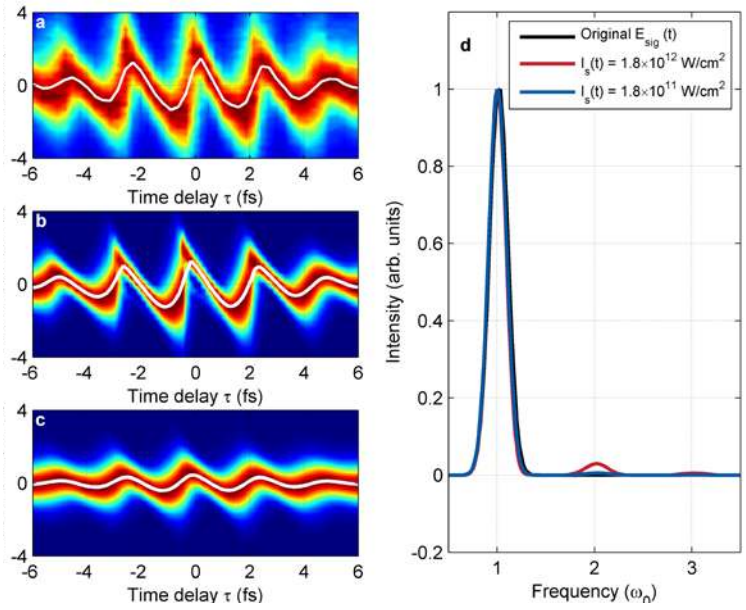

Figure S3: **Distortion of the measured waveform a,** The waveform measured in the experiment (Fig. 3b in the manuscript). **b-c,** The calculation results obtained with the SFA model. The harmonic emissions generated from a single re-collision are calculated from Ne atoms distributed in 1-D. The intensity of the fundamental driving pulse is 3.5×10^{14} W/cm^2. The color map shows the far-field angular distribution at 49 eV with a signal intensity of 1.8×10^{12} W/cm^2 (b) and 1.8×10^{11} W/cm^2 (c). **d,** The spectrum calculated from the original pulse, (b) and (c) are shown.

3.3 Two-source experiments

We have used the non-collinear geometry to measure the phase shift imposed by the signal field. The phase shift can also be measured by different experiment setup such as two XUV source experiments [3, 5, 6, 7]. In these experiments, two identical XUV beams are generated by two fundamental laser pulses. The signal pulse can be collinearly added in one of two laser beams. The phase shift can be obtained by measuring the shift of the fringe pattern at the far-field. Since the signal pulse can be added collinearly, the measurement will not surfer from the higher order distortion of the XUV wavefront.

References

[1] M. Lewenstein, P. Salières, and A. L'Huillier, "Phase of the atomic polarization in high-order harmonic generation," *Phys. Rev. A*, vol. 52, no. 6, p. 4747, 1995.

[2] N. Dudovich, O. Smirnova, J. Levesque, Y. Mairesse, M. Y. Ivanov, D. M. Villeneuve, and P. B. Corkum, "Measuring and controlling the birth of attosecond xuv pulses," *Nature Physics*, vol. 2, no. 11, pp. 781–786, 2006.

[3] D. R. Austin, T. Witting, C. A. Arrell, F. Frank, A. S. Wyatt, J. P. Marangos, J. W. G. Tisch, and I. A. Walmsley, "Lateral shearing interferometry of high-harmonic wavefronts," *Opt. Lett.*, vol. 36, no. 10, pp. 1746–1748, 2011.

[4] K. T. Kim, C. Zhang, A. D. Shiner, S. E. Kirkwood, E. Frumker, G. Gariepy, A. Naumov, D. M. Villeneuve, and P. B. Corkum, "Manipulation of quantum paths for space-time characterization of attosecond pulses," *Nature Physics*, vol. 9, pp. 159–163, 2013.

[5] Y. Mairesse, D. Zeidler, N. Dudovich, M. Spanner, J. Levesque, D. Villeneuve, and P. Corkum, "High-order harmonic transient grating spectroscopy in a molecular jet," *Phys. Rev. Lett.*, vol. 100, pp. 143903–1, 2008.

[6] J. B. Bertrand, H. J. Wörner, P. Salières, D. M. Villeneuve, and P. B. Corkum, "Linked attosecond phase interferometry for molecular frame measurements," *Nature Physics*, vol. 9, pp. 174–178, 2013.

[7] O. Smirnova, Y. Mairesse, S. Patchkovskii, N. Dudovich, D. M. Villeneuve, P. B. Corkum, and M. Y. Ivanov, "High harmonic interferometry of multi-electron dynamics in molecules," *Nature*, vol. 460, no. 7258, pp. 972–977, 2009.